Investigation of the elementary mechanisms controlling dislocation/twin boundary interactions in fcc metals and alloys: from conventional to advanced TEM characterization

H. Idrissi and **D. Schryvers**

EMAT, University of Antwerp, Groenenborgerlaan 171, B-2020 Antwerpen, Belgium

The elementary mechanisms controlling the interactions between lattice gliding dislocations and twin boundaries were carefully analyzed using conventional and advanced transmission electron microscopy techniques in both bulk coarse-grained Fe-Mn-C TWIP steels with deformation twins and nanocrystalline Palladium thin films with nanoscale growth twins. The results reveal that the individual dislocation/TB reactions depend mainly on the stacking fault energy of the material as well as the nature of the incoming dislocations nucleated during the plastic deformation of the material. It is also demonstrated that such investigation requires dedicated and specific microscopic techniques depending on the microstructure and the intrinsic properties of the crystallographic defects of the materials.

Keywords coarse-grained materials; nanocrystalline materials; plastic deformation; dislocation; twin boundary

1. General introduction

Twin boundaries (TBs) in face centered cubic (fcc) metals and alloys can be categorized into deformation, annealing, and growth twins. These low-energy planar interfaces, which exhibit exceptional mechanical and thermal stability were the subject of several studies in the past because of their beneficial effect on the mechanical behavior of these materials. Recently, there is a strong renewed interest on these defects motivated by the recent development of new synthesis techniques capable to produce bulk and small fcc systems with well controlled populations of nanoscale twins.

Deformation twinning in fcc coarse-grained metals has been studied extensively in the past and recently reviewed by Christian and Mahajan [1]. All these studies have revealed that the twinning tendency is largely determined by the stacking fault energy (SFE) of the metal. For example, coarse-grained fcc metals with high SFEs such as Al and Ni normally deform by dislocation slip, while fcc metals with low SFEs such as Ag primarily deform by twinning [2,3]. Based on this result, new and innovative strategies were thus developed for the enhancement of the deformation twinning tendency in fcc coarse-grained metals. The most evident route is the use of alloying elements in these materials for lowering of the SFE and the resulting enhancement of deformation twinning.

Recently, bulk nanocrystalline (nc) metals which can be defined as solids with grain sizes in the range of 1–100 nm were successfully synthesized by either two-step approaches such as nano-powder synthesis and consolidation [4], or one-step approaches such as severe plastic deformation [5]. Furthermore, following the observation of deformation twinning in bulk nc metals, even in high SFE metals such as Al [6], there has been significant interest in studying twinning as a deformation mode in these materials.

Another important breakthrough is the fabrication of fcc metallic thin films and layers with nanotwinned structures using methods such as electro-deposition [7] or sputter deposition [8]. Nanotwinned fcc metals made via sputtering can have twin boundary (TB) spacings as small as 2–4 nm and preferential alignment of {111} TBs normal to the growth direction [8]. These as-grown nanotwinned structures exhibit unusual properties as compared to the above mentioned nc metals. Typically, in nc metals with high-angle grain boundaries (GBs) the increased strength is accompanied by a loss in ductility, thermal stability, and electrical conductivity. However, nanotwinned metals such as copper exhibit very high tensile strengths, with good ductility, thermal stability, and electrical conductivity at room temperature [7].

It is worth mentioning that during the plastic deformation of the coarse-grained or nc materials, the interactions between lattice perfect or partial dislocations with both growth and deformation TBs are inevitable. Such reactions, which are expected to control the mechanical behavior of the twinned systems, have been observed both experimentally [7,9,10] and by molecular dynamic (MD) simulations [11-13]. Twins are believed to be effective in simultaneously increasing the strength and the ductility by acting as obstacle for lattice deformation dislocations as well as sources for dislocation multiplication and storage via specific reactions between twins and lattice gliding dislocation at the twin/matrix interfaces [7]. However, the fundamental mechanisms controlling the dislocation/TB reactions are still under debate since these reactions are complex and affected by several parameters such as the SFE of the material, the properties of the dislocations involved in the reactions, the presence of impurities, etc. Moreover, the investigations of dislocation/TB reactions have not yet benefited much from new advanced transmission electron microscopy (TEM) techniques such as aberration corrected microscopy, able to provide unique information at the nanoscale.

In the present paper, both conventional and advanced TEM techniques were used to unravel the fundamental processes governing the interaction of lattice dislocations with deformation twins in bulk coarse-grained Fe-Mn-C TWIP (twinning-induced plasticity) steels as well as with growth nanoscale twins in nc Pd thin films produced by electron beam evaporation. The paper also reports the evolution and the adaptability of the TEM techniques available nowadays for the study of the dislocation/TB interactions in materials exhibiting different microstructural properties (grain size, stacking fault energy, alloying elements, etc). This experimental approach will be of great importance for the understanding of the mechanical behaviour of twinned materials and will yield new data for the continuously growing efforts for the modelling of these reactions.

2. Dislocation/TB reactions in coarse-grained Fe-Mn-C TWIP steels

For several years now, focused studies have been carried out on what is called "twinning-induced plasticity" steels. The acronym "TWIP" came after the similar "TRIP" acronym, which stands for transformation-induced plasticity, to designate a new generation of advanced high-strength steels. It corresponds to specific Fe–Mn steel grades in which mechanical twinning occurs and leads to a large strength–ductility balance thanks to an enhanced work hardening rate. Such behaviour has been used for a very long time in Fe-Mn-C Hadfield steels, which were named after the work of R.A. Hadfield [14]. However, despite several decades of research, the real origin of the large work hardening rate exhibited by these steels remains partially unclear and a matter of debate. Also, in the literature, hardly anything can be found on the TEM investigation of dislocation/TB interactions expected to affect strongly the mechanical behaviour of these materials. It is thus the aim of the present study to elucidate the origin of the elevated work-hardening rate of Fe–Mn–C TWIP steels based on the investigation of these reactions.

2.1 Materials and experimental procedures

The chemical composition of the investigated Fe–Mn–C austenitic TWIP steels is Fe–20 wt.% Mn–1.2 wt.% C. Cast ingots were hot rolled down to 3.5 mm in thickness, then cold rolled to either 1.5 or 1 mm thick sheets. Recrystallization annealing was finally conducted prior to mechanical testing and microstructural characterization. Tensile specimens were then strained to different levels up to fracture at room temperature. A huge uniform strain and true stress at the onset of necking was observed resulting from a large hump in the evolution of the work-hardening rate with strain [15].

Prior to the TEM observations, disks 3 mm in diameter were machined by electrical discharge machining from the strained samples. Electron transparent areas were obtained by twin-jet electropolishing with a solution of 5% HClO4 and 95% acetic acid at room temperature. A Philips (LaB_6, CM20) transmission electron microscope operating at 200 kV was used for the observations. The character and the morphology of the extended defects (SFs and dislocations) were identified using the bright-field (BF) technique in two-beam diffraction condition. In the next section, it will be also shown that different dislocation components, i.e. perfect dislocations, Frank sessile dislocations and Shockley partial dislocations (SPDs), are involved in the reactions between the lattice dislocations and the deformation TBs. In order to characterize these dislocations, careful TEM examinations were carried out based on both the dislocation geometry and the invisibility criterion $\boldsymbol{g}.\boldsymbol{b}=0$. This last condition was used in BF two-beam condition to identify perfect dislocations with Burgers vector of type $\boldsymbol{b}=\frac{a}{2}\langle 110\rangle$. Furthermore, SPDs with Burgers vector $\boldsymbol{b}=\frac{a}{6}\langle 112\rangle$ and bounding SFs can be invisible when $\boldsymbol{g}.\boldsymbol{b}$ is small, but not necessarily zero. It is also generally argued that SPDs are invisible for $|\boldsymbol{g}.\boldsymbol{b}|\leq\frac{1}{3}$. SFs are invisible when the displacement vector $\boldsymbol{R}=\frac{a}{3}\langle 111\rangle$ is perpendicular to the diffraction vector $\boldsymbol{g}$ ($\boldsymbol{g}.\boldsymbol{R}=0$). The two-beam dynamic theory originally presented by Howie and Whelan [16] and then modified by Silcock and Tunstall [17] was used to identify Frank partial dislocations since these dislocations exhibit an anomalous diffraction contrast. Indeed, Silcock and Tunstall [17] proposed the extended invisibility criteria based on their calculation of intensity profiles considering anomalous electron absorption effects (two-beam dynamic theory). They reported that the Frank partials exhibit a so-called "reversal of contrast" under 002 and $00\bar{2}$ reflections. For example, a Frank partial dislocation with Burgers vector $\boldsymbol{b}=\frac{a}{3}[111]$ will be visible with $\boldsymbol{g}$=002 ($\boldsymbol{g}.\boldsymbol{b}=+\frac{2}{3}$) but out of contrast with $\boldsymbol{g}=00\bar{2}$ ($\boldsymbol{g}.\boldsymbol{b}=-\frac{2}{3}$) in contradiction with the original criteria of Howie and Whelan [16] (all the partial dislocations with $\boldsymbol{g}.\boldsymbol{b}=\pm\frac{2}{3}$ should be visible irrespective of their plus or minus sign). In the original paper of Silcock and Tunstall [17], the "reversal of contrast" was observed only for a dimensionless parameter $W=\xi_g s_g$ above 0.3 (with ξ_g being the extinction distance for the 002 reflection, and s_g the deviation parameter extracted from the diffraction data). It was also reported by Silcock and Tunstall [17] that the $\frac{a}{3}[111]$ Frank dislocations give a characteristic strong oscillatory contrast when using the $\boldsymbol{g} = 2\bar{2}0$ reflection although the value of the product ***g***.***b***=0 is zero. This condition will also be used to identify Frank dislocations in the present study.

2.2 Results and discussion

The average grain size of the Fe-Mn-C TWIP steels under study was measured using the electron back scattered diffraction (EBSD) technique and found to be around 15 µm. Conventional diffraction contrast imaging was thus used to investigate the extended defects within the large grains. Also, due to the large work hardening capacity of the Fe-Mn-C, the number of the dislocations stored within the grains was quite elevated even for small deformation levels. This makes the analysis of individual extended defects very difficult using high resolution TEM (HRTEM).

Figure 1 presents three micrographs obtained with different two-beam diffraction conditions in Fe-Mn-C sample deformed to ε = 0.02. This figure exhibits one planar defect corresponding to wide overlapping SFs bounded by partial dislocations, and thus considered as a twinning precursor. Details on the investigation of the nucleation process of these precursors are given in [15]. The present paper only focuses on the interaction between deformation lattice dislocations with pre-existing deformation or growth twins. It is worth mentioning here that, by tilting the region shown in Fig. 1, it was confirmed that the exact twinning plane for the twin precursor corresponds to the $(\bar{1}\bar{1}1)$ plane [15]. In Fig. 1, a curved dislocation line separating two different faulted regions in the twinning plane is indicated by a white arrow. This dislocation corresponds to a twinning SPD gliding in the $(\bar{1}\bar{1}1)$ twinning plane and dragging a wide SF behind it. This dislocation is out of contrast with ***g***=002, ***g*** =111 and ***g***=200, even though it presents a small residual contrast in Fig. 1a (corresponding to ***g***=002). In the $(\bar{1}\bar{1}1)$ twinning plane the unique SPD that satisfies the extinction condition ($|\boldsymbol{g}.\boldsymbol{b}| = \frac{1}{3}$) with the three reflecting planes considered in Fig. 1 is the $\boldsymbol{b} = \frac{a}{6}[\bar{1}21]$ partial.

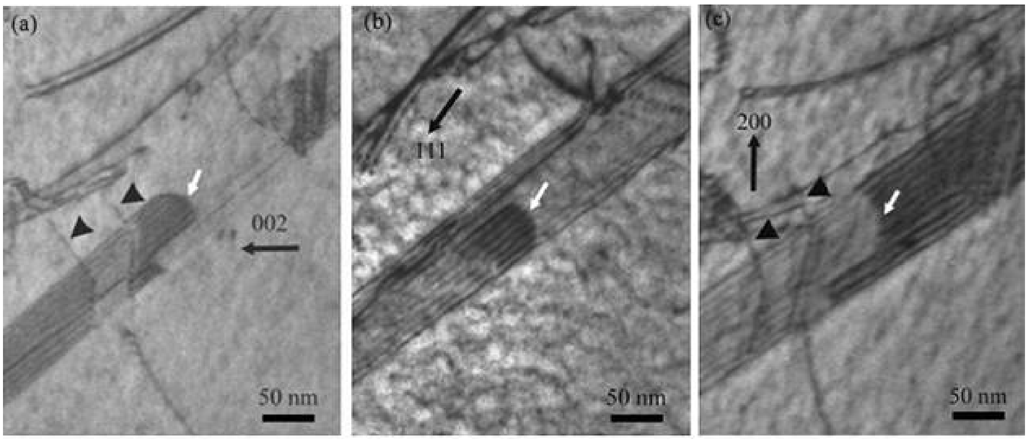

Fig. 1 Shockley partial dislocation in the twinning plane observed with (a) ***g***=002, (b) ***g*** =111 and (c) ***g*** =200.

The BF micrograph of Fig. 2a, obtained with the reflecting plane ***g***=002, shows other details on the twinning precursors. Straight parallel dislocations associated with the overlapping SFs can be clearly observed. These dislocations retain their straight morphology when the sample is tilted. They are thus not influenced by the applied shear stress during deformation. These straight dislocations are parallel to the $[1\bar{1}0]$ direction, which corresponds to the intersection between the (111) and $(\bar{1}\bar{1}1)$ close-packed planes. They can thus correspond to:

(i) Sessile stair-rod dislocations formed by the stair-rod cross-slip mechanism proposed by Mori and Fujita [18] with the dissociation of $\boldsymbol{b} = \frac{a}{6}[\bar{2}11]$ SPD lying initially in the (111) primary plane into a stair-rod dislocation with the Burgers vector $\boldsymbol{b} = \frac{a}{6}[\bar{1}\bar{1}0]$ and another Shockley partial dislocation in the $(\bar{1}\bar{1}1)$ conjugate twinning plane with $\boldsymbol{b} = \frac{a}{6}[\bar{1}21]$ (analysed experimentally in Fig. 1) following:

$$\frac{a}{6}[\bar{2}11]_{(111)} \rightarrow \frac{a}{6}[\bar{1}\bar{1}0]_{Sessile} + \frac{a}{6}[\bar{1}21]_{(\bar{1}\bar{1}1)} \quad (1)$$

In this case, the $\boldsymbol{b}=\frac{a}{6}\left[\bar{2}11\right]$Shockley partial dislocation in the reaction (1) can be obtained by the dissociation of a $\boldsymbol{b}=\frac{a}{2}\left[\bar{1}01\right]$ perfect dislocation in the (111) primary plane following:

$$\frac{a}{2}\left[\bar{1}01\right]_{(111)} \rightarrow \frac{a}{6}\left[\bar{1}\bar{1}2\right]_{(111)} + \frac{a}{6}\left[\bar{2}11\right]_{(111)} \tag{2}$$

The micrographs of Fig. 2b, obtained with the reflecting plane ***g***=202, show pile-ups of narrowly dissociated dislocations (marked by black arrowhead) that interact with the twinning precursor. SF fringes on another plane than the twinning plane associated with the SPDs can also clearly be seen. In this case, the exact Burgers vector of the SPDs could not be determined, since the microscope goniometer stage reached its tilt limit. However, from the orientation of the SF fringes, it can be determined that the SPD lies in the (111) plane. It can thus be postulated that they correspond to the $\boldsymbol{b}=\frac{a}{6}\left[\bar{1}\bar{1}2\right]$ and $\boldsymbol{b}=\frac{a}{6}\left[\bar{2}11\right]$ Shockley partial dislocations resulting from the dissociation given in the reaction (2).

(ii) Sessile Frank dislocations generated by the pole mechanism with the deviation process proposed by Cohen and Weertman [19], with the dissociation of a $\boldsymbol{b}=\frac{a}{2}\left[\bar{1}01\right]$ perfect dislocation in the (111) primary plane into a Frank sessile dislocation and the observed $\boldsymbol{b}=\frac{a}{6}\left[\bar{1}21\right]$ SPD in the $(\bar{1}\bar{1}1)$ conjugate twinning plane following:

$$\frac{a}{2}\left[\bar{1}01\right]_{(111)} \rightarrow \frac{a}{3}\left[\bar{1}\bar{1}1\right]_{Sessile} + \frac{a}{6}\left[\bar{1}21\right]_{(\bar{1}\bar{1}1)} \tag{3}$$

Since perfect dislocations observed in the matrix were found to be dissociated into SPDs (Fig. 2b), the reaction (3) requires the constriction of the SF and the recombination under the applied stress of the two Shockley partials of the reaction (2) when meeting the TB.

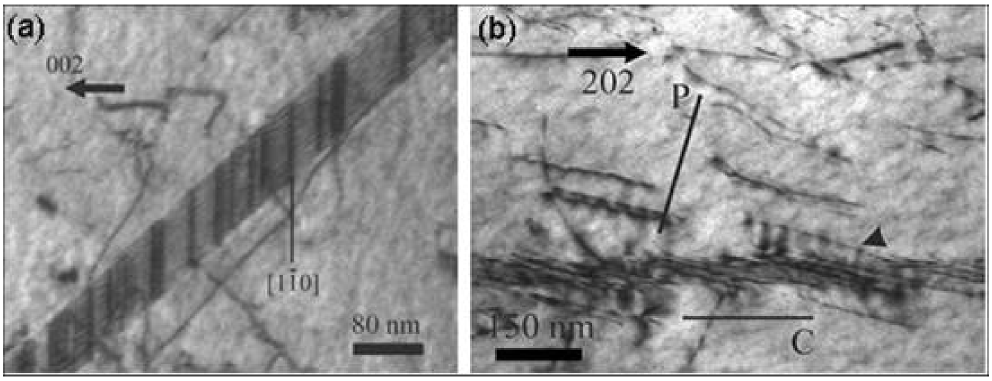

Fig. 2 (a) Straight sessile dislocations parallel to the $\left[1\bar{1}0\right]$ direction observed with ***g***=002. (b) Dissociated Shockley partials interacting with the twin precursor observed with ***g***=202. "P" and "C" indicate the position of the primary and the conjugate twinning plane.

In order to discriminate between the two potential mechanisms in the present case (i.e. the stair-rod cross-slip mechanism [18] or the "pole + deviation" mechanism [19]), the distinction between Frank and stair-rod dislocations was considered in more detail by considering the "reversal of contrast" exhibited by Frank dislocations under the two opposite reflecting planes $\boldsymbol{g}=002$ and $\boldsymbol{g}=00\bar{2}$ with varying *W*, according to the modified two-beam dynamic theory proposed by Silcock and Tunstall [17]. Figure 3 shows a series of BF micrographs obtained with $\boldsymbol{g}=00\bar{2}$ and $\boldsymbol{g}=002$ on the straight dislocations related to the twinning precursors and expected to be stair-rod or Frank dislocations.

In the micrographs of Figs. 3a and b, the straight dislocations exhibit similar contrast under $\boldsymbol{g}=00\bar{2}$ and $\boldsymbol{g}=002$ when $W=0$. However, in Figs. 3c and d, corresponding to $W=0.7$, the straight sessile dislocations are visible with $\boldsymbol{g}=00\bar{2}$ but disappear with $\boldsymbol{g}=002$. In Fig. 3d, although the change in fringe position still yields some residual contrast, the extinction is clearly visible for the two dislocations shown by arrowheads. This result confirms that the sessile dislocations correspond to Frank dislocations in agreement with the results obtained by Silcock and Tunstall [17]. In addition, the sessile dislocations expected to be a $\frac{a}{3}\left[\bar{1}\bar{1}1\right]$ Frank dislocations exhibit, in Fig. 2b, a strong contrast with

$\boldsymbol{g} = 202$ parallel to the twinning plane although $\boldsymbol{g}.\boldsymbol{b}$=0, which is a characteristic of Frank dislocations as also reported by Silcock and Tunstall [17].

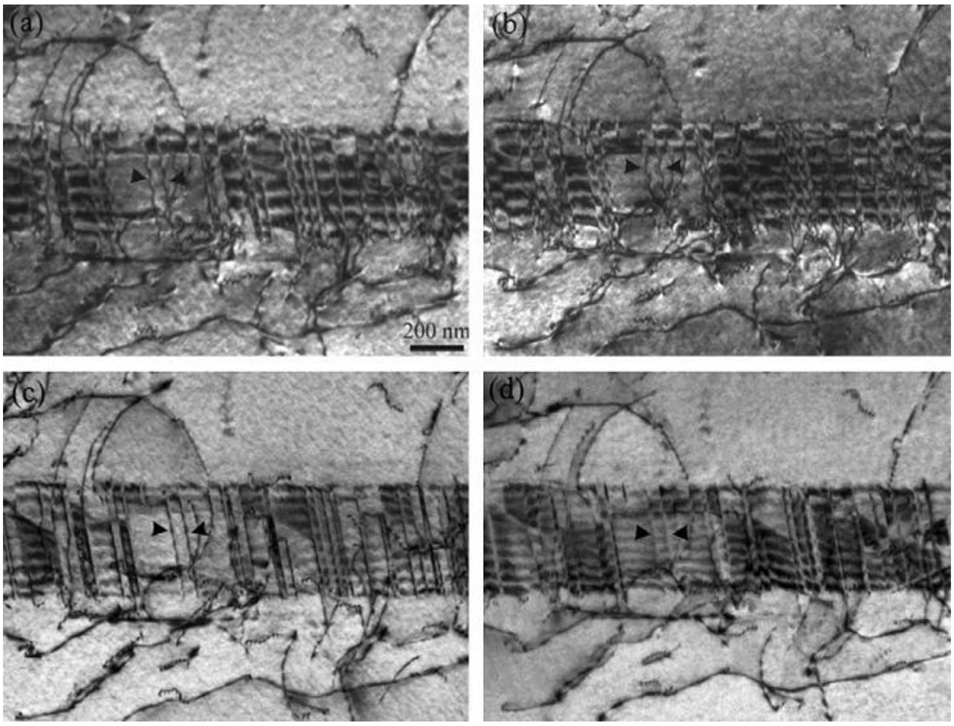

Fig. 3 BF micrographs obtained under (a) $\boldsymbol{g} = 00\bar{2}$ with $W = 0$, (b) $\boldsymbol{g} = 002$ with $W = 0$, (c) $\boldsymbol{g} = 00\bar{2}$ with $W = 0.7$ and (d) $\boldsymbol{g} = 002$ with $W = 0.7$.

Based on these results, the pole mechanism with deviation proposed by Cohen and Weertman [19] is fully compatible with the dislocations and extended defects observed here. This mechanism can be summarized as follows. Under the applied stress, a $\frac{a}{2}\left[\bar{1}01\right]$ perfect dislocation in the matrix primary plane dissociates when meeting the TB, into a $\frac{a}{3}\left[\bar{1}\bar{1}1\right]$ Frank sessile dislocation located at the intersection of the primary and conjugate planes and a $\frac{a}{6}\left[\bar{1}21\right]$ Shockley partials, now gliding in the conjugate twinning plane, following the reaction (3). In Figs. 1a and c, two perfect dislocations connected to Frank sessile dislocations are indicated by black arrowheads confirming the dissociation process of reaction (3). These dislocations are invisible in Fig. 1b.

Figure 4 illustrate the mechanism controlling the dislocation/TB reactions in Fe-Mn-C TWIP steels as concluded from the TEM observations. The pileups of extended dislocations in the primary plane interact with the TBs with the systematic formation of Frank dislocations at the intersection sites between the primary and the conjugate plane. The SFE of the present steel is not low enough to avoid the constriction of SFs in the primary plane under the applied stress (15 $mJ.m^{-2}$ as measured in [15]). As a consequence, the two partials of reaction (2) recombine under the applied stress when meeting the TB. Thus, the perfect dislocation is totally incorporated at the TB, followed by the dissociation of reaction (3), with the production of Frank sessile dislocations and Shockley dislocations in the twinning plane.

Based on these results, it is clear that that the activation of the “pole + deviation” mechanism in Fe-Mn-C will influence both the thickness of the twins and the resistance of the TBs for the penetration of lattice dislocations, elevating thus the work hardening rate. On the one hand, due to the presence of a huge density of sessile Frank dislocations at the twin/matrix interfaces (Fig. 2a), the mobility of the SPDs lying in the twinning plane will be certainly affected and the thickening of the twins reduced. On the other hand, the sessile dislocations will act as strong obstacles for further incoming lattice dislocations hampering thus the interaction of these dislocations with the TBs. Details concerning the consequences of such features on the mechanical behaviour of Fe-Mn-C TWIP steels can be found in [15].

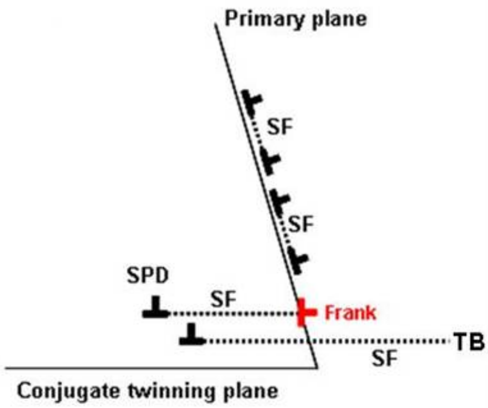

Fig. 4 Illustration of the dislocation/TB reactions in Fe-Mn-C TWIP steels

3. Dislocation/TB reactions in nanocrystalline Pd thin films

Nc thin metallic films suffer from a lack of ductility, which limits their use in a variety of applications involving flexible electronics, MEMS, microelectronics, and thin functional coatings [20-22]. Ductility is directly connected to the ability of a material to deform plastically without plastic localization or without damage. Often the limited resistance to plastic localization is the main concern in thin films [23]. The resistance to plastic localisation is inherently related to the strain hardening capacity, i.e. the capacity of metals to harden with plastic deformation. Same as for nanostructured bulk metallic materials, the strain hardening capacity of thin metallic films is often very low, explaining the weak ductility. The reasons for the low strain hardening capacity essentially relate to the absence of forest hardening mechanisms when the grain size is in the submicron range.

Recently, we investigated ~25 nm grain size Pd thin films containing coherent growth TBs [24] deformed using a novel concept of an on-chip nanomechanical testing stage [25]. An unexpected large strain hardening capacity compared to what is currently reported for nc metallic thin films was observed leading to fracture strains as large as 8% in some specimens and more than 1 GPa strength. This large strength/ductility balance was partly attributed to the presence of nanotwins providing an isotropic hardening contribution to the strain hardening capacity [24].

The aim of the present paper is thus to present a detailed TEM analysis of the dislocation/TB reactions in Pd films to elucidate their contribution on these remarkable mechanical properties. The results can be used for further enhancement of the ductility of Pd films as needed for instance in Pd-based membranes in hydrogen applications [26].

3.1 Materials and experimental procedures

The Pd films were deposited by electron-beam evaporation on top of a 5 nm thick Cr layer to ensure proper adhesion to the substrate (see details in [24,27]). The temperature of the substrate was limited to 100°C. Pd films with thickness of 310, 160 and 80 nm have been tested using a recently developed on-chip testing method [25]. The basic idea of this technique devoted to the testing of submicron freestanding films is to use internal stresses introduced in a long actuating beam to deform another material attached to it by removing the underneath sacrificial layer. The details about the technique, the design rules and its range of applications are given elsewhere [24,25,27].

In order to uncover the mechanism(s) controlling the interactions of the lattice gliding dislocations with TBs, TEM have been extensively used to characterize the evolution of the microstructure in the Pd thin films before and after deformation. These in-depth TEM characterizations were mostly performed on the 310 nm thick films. Conventional Bright field BF and Dark field (DF) TEM characterization was carried out with a CM20 (LaB_6, 200 kV) microscope to observe the overall microstructure at low TEM magnification (grain size, twins,…) while HRTEM was used to determine the properties of the crystallographic defects at the nanoscale in a TECNAI G2 (Field Emission Gun, 200kV) microscope. Proper analysis of the mechanism(s) controlling the dislocation/TB reactions has also required the investigation of the dislocation cores. However, some of these dislocations exhibit strong strain field contrast in conventional HRTEM images that masks the information on the defect core. On top of the adverse effect of the strain field contrast, the resolution of non-aberration corrected electron microscopy is, in some instances, insufficient to image the intricate details of a dislocation. To overcome these two issues, aberration-corrected high resolution scanning TEM (HRSTEM) was adopted instead of conventional HRTEM to reveal the near-core properties of dislocations at the nanoscale [28]. These HRSTEM experiments were carried out on a FEI Titan 80-300 “cubed” microscope fitted with an aberration-corrector for the imaging lens and the probe forming lens as well as a monochromator, yielding a resolution in STEM mode around 80 pm. An Annular Dark Field (ADF) camera length of 286 mm (detector inner semi-angle of ~16 mrad) was selected to allow some diffraction contrast on the ADF detector in order to easily recognize the dislocations.

3.2 Results and discussion

Figure 5 shows BF micrograph on cross-sectional TEM samples prepared by focused ions beam (FIB) technique from 310 nm thick as-deposited Pd films. This figure show that the Pd thin films exhibit a morphological texture with columnar grains elongated parallel to the growth direction. The ring shaped selected area diffraction pattern (SADP) shown in the upper right of Fig. 5 reveals the fcc Pd crystalline structure. No clear preferential crystallographic orientation of the grains is detected from the SADP of Fig. 5, indicating the absence of a marked crystallographic texture. The statistical distribution of the in-plane grain size and of the aspect ratio of the grains (grain height / in plane grain size) in the as-deposited films yields an average grain diameter of 25.6±7.3 nm with an aspect ratio equal to ~7. Around 200 grains were included in the analysis.

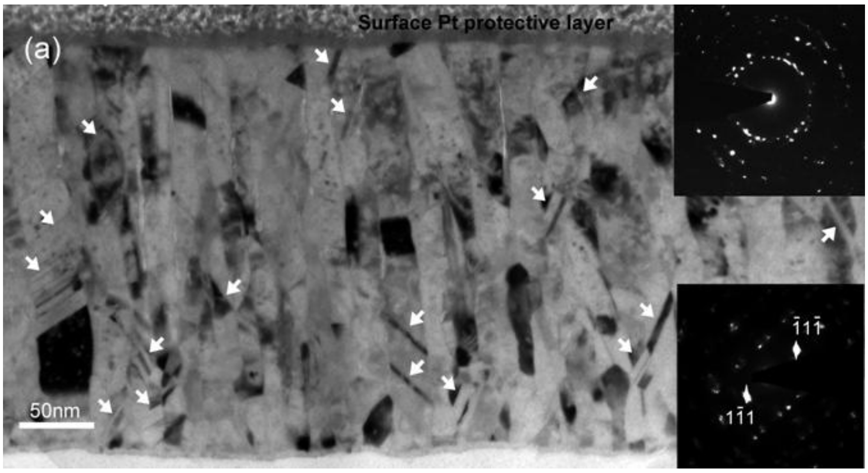

Fig. 5 BF micrographs obtained in cross-sectional FIB samples before deformation of 310 nm thick Pd films

A significant density of planar defects was observed inside the grains of the as-deposited Pd films as indicated by white arrows in the BF micrograph of Fig. 5. These defects were identified as $\{111\}$ nanotwins using the nanodiffraction pattern provided in the lower right part of Fig. 5. Indeed, the diffraction pattern obtained from a TB region and oriented along a $\langle 110\rangle$ zone axis reveals the typical superposition of two mirrored $\langle 110\rangle$ diffraction patterns with respect to the $\{111\}$ plane. Figure 5 also shows that most twins are not parallel to the surface of the film and that their orientation changes randomly from one grain to another, confirming the absence of clear crystallographic texture. The twins are heterogeneously distributed within the grains and over the film thickness. The distance between two subsequent TBs ranges from 1~2 nm to 20 nm. About 20% to 30% of the grains are estimated to contain 1 or 2 TBs in the as-deposited films. It important to note here that, due to the small grain size shown in Fig. 5 defect analysis using conventional TEM proved to be very difficult. Thus, HRTEM was used to investigate the dislocation/TB interactions in the Pd films.

Figure 6a shows a HRTEM image of one nanograin with a lateral diameter of 21 nm, containing a 1.3 nm thick growth twin observed in the as-deposited Pd film. The TBs in Fig. 6a are perfectly coherent and atomically sharp without steps and any residual dislocations located at the TB. This result was confirmed by further HRTEM analysis of several TBs in the as-deposited films. Furthermore, the grain of the Fig. 6a does not reveal significant dislocation activity. Indeed, the HRTEM image of this figure exhibits a homogenous contrast free from dislocations. Only one dislocation in the upper left part of Fig. 6a can be observed (see the high magnification insert). Although this dislocation is located at the vicinity of one of the TBs, it does not correspond to a twinning SPD because the extra half plane of the dislocation does not terminate at the twinning plane.

Figure 6b shows a HRTEM micrograph of a Pd film subjected to 4% deformation. This image exhibits a long grain with one growth TB almost parallel to the film surface. Careful analysis of the TB, magnified in Fig. 6c, shows that, contrary to the HRTEM images of Fig. 6a, the TB of Fig. 6b has lost coherency. Indeed, the atomic structure of this TB exhibits severe distortions associated to strongly inhomogeneous strain fields. Coherent TBs are characterized by their thermal and mechanical stability compared to GBs. Shearing along coherent TBs is thus extremely difficult. Interactions of gliding dislocations in the crystal lattice with the TBs must thus be invoked to explain the observed loss of coherency of the TBs. This scenario is in agreement with the strong variations of the average contrast related to a high local density of dislocations observed in the grain of Fig. 6b. Some of these dislocations are indicated in the micrograph of Fig. 6b. They were probably nucleated from GBs during the plastic deformation of the films. Other HRTEM analyses of Pd films before and after the release step show similar results, confirming that the Pd films deform by the activation of slip systems inside the grains.

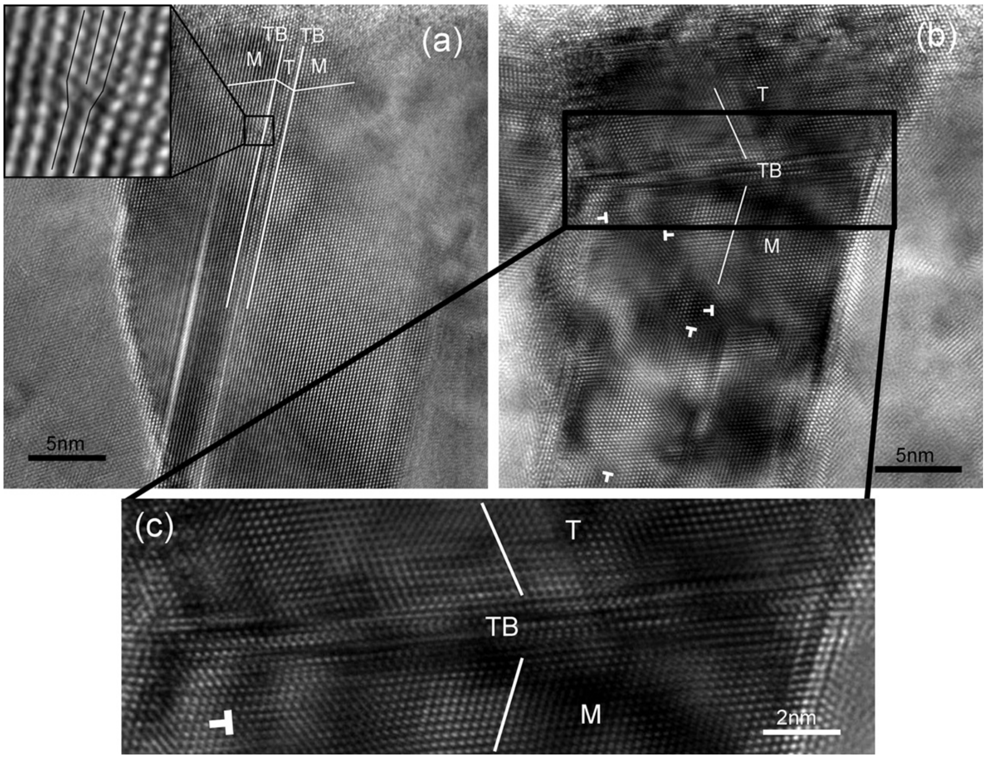

Fig. 6 HRTEM images obtained in (a) as-deposited and (b,c) 4% deformed 310 nm thick Pd films.

A careful investigation of individual dislocations lying at the twin/matrix interfaces has been carried out using HRTEM. For this purpose Pd films subjected to moderate strain were selected, in order to avoid the large distortion of the atomic structure of the TB observed at large strains (Fig. 6c). Figure 7 is a HRTEM micrograph of a single TB in a Pd film subjected to 0.8% deformation.

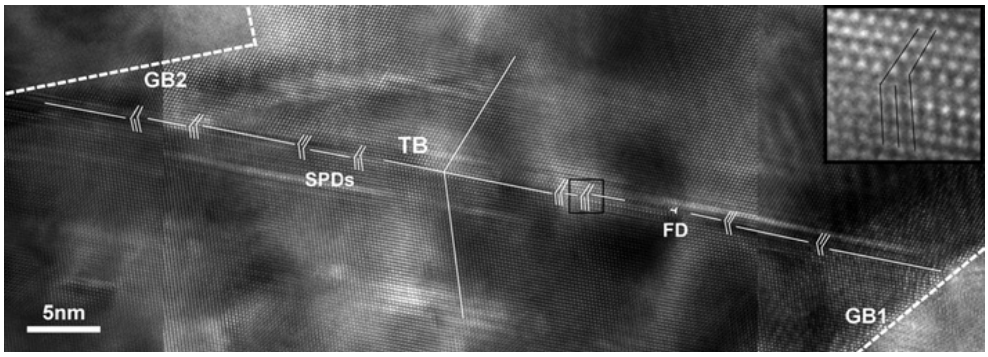

Fig. 7 HRTEM image of a single TB in a Pd films deformed at 0.8%; 8 SPDs and only one Frank dislocation (FD) can be observed at the twin/matrix interface.

In this image, distinct atomic steps can be observed along the TB. These steps are due to the presence of several SPDs dragging large SFs in the twinning plane. The locations of the extra half planes related to these SPDs are indicated in Fig. 7. This figure also reveals strong local residual contrast related to one sessile dislocation located at the TB. This strain contrast hampers the investigation of the dislocation core and whether it is connected to other defects (e.g., in the case of stair-rod sessile dislocation, a short SF connected to the TB and located in the matrix or in the twinned region).

Figure 8 is a micrograph obtained by aberration-corrected high resolution ADF-STEM on the 0.8% deformed sample, showing two sessile dislocations located at two parallel TBs. The dark contrast originating from the strain field surrounding the core of the sessile dislocation in Fig. 7 is highly decreased and could be minimized even more by reducing the ADF camera length to the high angle ADF (HAADF) regime. Here, however, an ADF camera length (ADF detector inner semi-angle of ~16 mrad) was used to allow enough diffraction contrast in the image in order to easily locate the dislocations and to provide a higher signal-to-noise ratio in the images at minimal dwell times.

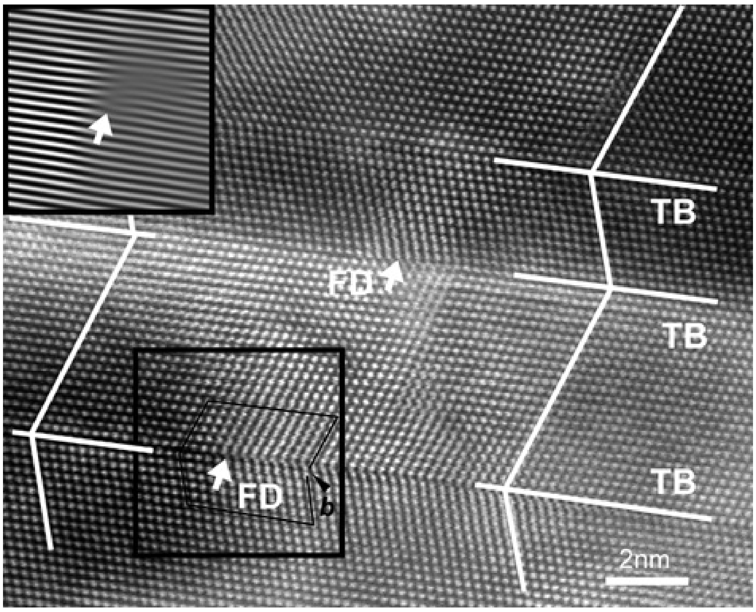

Fig. 8 High resolution STEM image of two parallel TBs in Pd film deformed at 0.8%. Two Frank sessile dislocations located at the TBs can be distinguished. The strain field contrast related to Frank sessile dislocations is lowered by using ADF-STEM while the resolution is severely improved compared to conventional HRTEM images. The exact position of the extra-half planes corresponding to the two Frank dislocations can be clearly observed. A Burgers circuit was drawn around the core of one Frank dislocation in order to determine its Burgers vector.

No SFs located in the matrix or in the twinned regions and connected to the sessile dislocations are observed in Fig. 8. It can thus be expected that these sessile dislocations correspond to Frank sessile dislocations instead of stair-rod dislocations. Inverse Fast Fourier Transformation (FFT) images obtained on the region containing one sessile dislocation in Fig. 8 reveal that the extra plane of this dislocation is parallel to the twinning plane. This result is in agreement with a Frank partial dislocation with Burgers vector of type $\frac{a}{3}\langle 111\rangle$. It also explains the shape of the strain field surrounding this type of dislocation in Fig. 7, which is characteristic of a dislocation with Burgers vector perpendicular to the twinning plane. Also, Fig. 8 shows the Burgers circuit drawn around the core of one Frank sessile dislocation and used to determine its Burgers vector. The measured value was found to be 0.224 nm, very close to the theoretical value of 0.223 nm for an edge $\frac{a}{3}\langle 111\rangle$ Frank dislocation. Further HRTEM observations of TBs in Pd films after deformation confirmed the presence of residual Frank sessile dislocations at the TBs. The origin of these dislocations can be attributed to the interaction of an extended dislocation with a coherent TB. For example, labeling the twinning plane in Fig. 7 as the $(1\bar{1}1)$ plane, a perfect dislocation of fcc Pd in the matrix plane $(1\bar{1}\bar{1})$ with a Burgers vector $\boldsymbol{b}=\frac{a}{2}[101]$ can nucleate from a GB under applied stress. When this extended dislocation is dissociated into two SPDs bounding a narrow SF following:

$$\frac{a}{2}[101]\rightarrow\frac{a}{6}[1\bar{1}2]+\frac{a}{6}[211] \tag{4}$$

the extended dislocation can interact with the coherent TB and dissociates owing to the applied stress into a $\boldsymbol{b}=\frac{a}{3}[1\bar{1}1]$ Frank sessile dislocation and a new $\frac{a}{6}[121]$ SPD in the $(1\bar{1}1)$ twinning plane following:

$$\frac{a}{2}[101]_{(1\bar{1}\bar{1})}\rightarrow\frac{a}{3}[1\bar{1}1]_{Sessile}+\frac{a}{6}[121]_{(1\bar{1}1)} \tag{5}$$

Since the SF energy of Pd is relatively high, the recombination of the two SPDs in the $(1\bar{1}\bar{1})$ plane following the reaction:

$$\frac{a}{6}[1\bar{1}2]+\frac{a}{6}[211]\rightarrow\frac{a}{2}[101] \tag{6}$$

does not require a very high stress. Recently, Jin et al. [29] used MD simulations to investigate the interactions between non-screw lattice dislocations and coherent TBs in pure fcc metals such as Cu, Ni and Al. For comparison with the present work the case of Al is the most relevant one because of a SFE similar to Pd (160-200 mJ.m^{-2} for Al, 100-180 mJ.m^{-2} for Pd). The simulations revealed that, depending on the Burgers vector of the incident dislocation and on the applied strain, the coherent TB may either allow complete slip transfer or act as a dislocation trap. Among the several possibilities of interactions in Al, the simulations predict the dissociation, under 3% applied strain, of a 60° incoming extended dislocation at the coherent TB into a Frank dislocation and a 30° SPD in the twinning plane, in agreement with the observation of Frank dislocations, partial twinning dislocations and perfect dislocations within the matrix in the present work (Figs 6b, 7 and 8).

Owing to the small grain size, most of the HRTEM images contain at least one individual grain (see e.g., Figs 6a and 6b). It was thus possible to precisely determine the total number and the nature of the dislocations located at TBs. In Fig. 7, the two opposite GBs limiting the single TB are labeled GB1 and GB2, and indicated by dashed lines. Furthermore, 8 SPDs can be identified along the TB, whereas only one Frank sessile dislocation is detected. Additional HRTEM observations confirmed that the number of SPDs in the twinning planes of moderately deformed grains is always larger than the number of Frank sessile dislocations. The dissociation reaction (5) cannot explain the excess of SPDs compared to Frank sessile dislocations, as observed in the present work (Fig. 7). Indeed, from this reaction, for one incident extended dislocation, one Frank dislocation will be produced at the TB, with the emission of one SPD in the twinning plane. In this case, identical numbers of Shockley twinning dislocations and Frank dislocations should be found along a TB (or even an excess of Frank sessile dislocations compared to glissile SPDs, the latter being possibly absorbed by the nearby GB). On the other hand, the large number of SPDs in the twinning plane cannot be attributed to the growth process, since, as demonstrated above, the TBs in the as-deposited films are perfectly coherent and do not contain any intrinsic defects (Fig. 6a). Also, the twin growth mechanism was attributed to a GB splitting mechanism instead of a twinning mechanism involving the nucleation and glide of SPDs [30]. Thus, another dislocation/TB interaction mechanism involving the formation of new SPDs in the twinning plane but without any residual defect at the twin/matrix interface should be invoked in order to explain the excess of SPDs compared to Frank dislocations observed in Fig. 7.

Jin et al. [29] have found also that under 4% applied strain, the Burgers vector of the 60° incoming extended dislocation is completely transferred across the TB. It dissociates at the coherent TB in three SPDs following the reaction:

$$\frac{a}{2}[101]_{matrix} \rightarrow \frac{a}{2}[101]_{twin} + \frac{a}{6}[121]_{twinning\_plane} \quad (7)$$

Two SPDs form a new extended dislocation with $\boldsymbol{b} = \frac{a}{2}[101]_{twin}$ gliding in the slip plane of the twin grain and a third one is a $\frac{a}{6}[121]$90° twinning partial which is left in the twinning plane. Due to the twin symmetry, the leading and trailing partials of the incoming dislocation exchange their order after the transmission. This mechanism does not involve the formation of a residual Frank sessile dislocation at the twin/matrix interface. It thus explains the excess of SPDs compared to Frank dislocations observed in Fig. 7.

Figure 9 summarizes the two most prominent mechanisms (labeled A and B) as concluded from the TEM observations to operate during the plastic deformation of the grains involving twins. It is worth repeating here that the high SFE of Pd will strongly affect the nature of the lattice dislocation/TB interactions. Indeed, the two reactions (5) and (7) involve the systematic constriction (under the applied stress) of the SF of the incident dislocation, followed by the recombination at the coherent TBs of the leading and the trailing SPDs. Additional contribution to the plastic deformation can be provided by the transmission of screw dislocations across coherent TBs via conventional stress-driven cross-slip. Indeed, due the high SF energy of Pd and the narrow splitting width between the partials, cross-slip could occur spontaneously when a screw dislocation enters the coherent TB. However, this process will not leave a visible signature for the ex-situ TEM imaging.

The dislocation/TB interaction mechanisms discussed here can partly explain both the high strength and the large strain hardening capacity of the Pd films. The presence of nanoscale TBs provides adequate barriers to dislocation motion. Indeed, TBs are considered as effective as conventional GBs in strengthening materials. However, dislocation glide is inhibited along GBs because of their disordered structure. Hence, the GBs have limited capacity to accommodate dislocations, resulting in a strength increase due to a Hall-Petch mechanism. The enhancement of the isotropic part of the strain hardening capacity owing to coherent TBs can be related to two different (but related) processes.

First, the coherent TBs offer multiple barriers to dislocation motion. In the present work, the efficiency of coherent TBs for trapping dislocations was confirmed experimentally by the observation of the sessile FDs possibly resulting from the dissociation reaction (5). According to this reaction, non-screw prefect dislocations can be dissociated when interacting with coherent TBs into residual Frank sessile dislocations at the TB, and SPD in the twinning plane. The accumulation at the TBs of Frank sessile dislocations with Burgers vectors out of the twinning plane produces a significant decrease of the TBs coherency (see Fig. 6c). Also, due to these sessile dislocations, mobile SPDs in the twinning plane could agglomerate during deformation and contribute to the decrease of coherency. The capacity of the TBs to stop the gliding dislocations can be expected to increase with the accumulation of Frank sessile dislocations at the interface, providing the strain hardening capacity. Second, TBs contribute to the increase of the work hardening by acting as sources for dislocation storage and multiplication. The excess of SPDs compared to Frank dislocations observed in Fig. 7 could be attributed to the complete slip transfer across TBs as predicted by reaction (7). The multiplication of dislocations is thus preserved via the storage of new SPDs in the twinning plane, and/or via the transmission of perfect dislocations from the matrix to the twin grain or vice versa. Other factors influencing the mechanical behavior of the Pd films under study are detailed in [31].

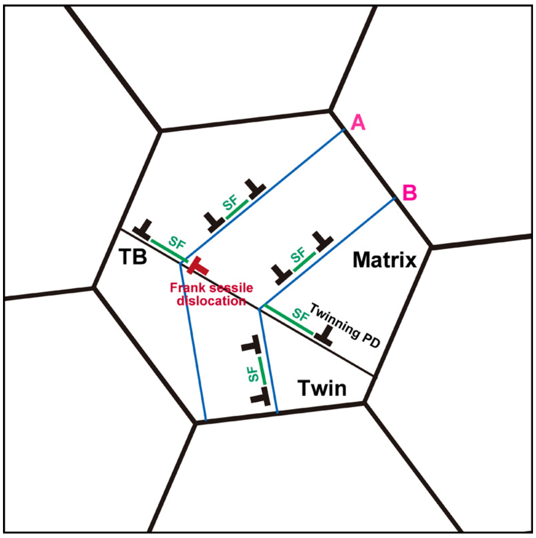

Fig. 9 Schematic illustration of the two mechanisms expected to control the lattice dislocation/coherent TB interactions in nanocrystalline Pd films with coherent growth twins; (A) dissociation of the incident dislocation into a Frank sessile and a Shockley twinning partial dislocation; (B) slip transfer of the incident dislocation across the coherent TB, with the emission of a new SPD in the twinning plane.

4. Conclusion

The fundamental processes governing the interaction of lattice gliding dislocations with both deformation and growth twins were investigated, respectively, in coarse-grained Fe-Mn-C TWIP steels and nc Pd thin films using conventional and advanced TEM techniques. The results show that several types of dislocations are involved in these reactions (e.g. perfect dislocations, Shockley partial twinning dislocations and residual Frank sessile dislocation at the TBs). The experimental TEM techniques used for the investigation of these dislocations can be categorized into two main groups depending mainly on the grain size:

i) For coarse-grained materials, the BF or DF two beam techniques with the standard extinction criterions can be used for the characterisation of perfect lattice dislocations and Shockley partials at the twinning plane. Frank sessile dislocations located at the TBs can be characterized using the “reversal of contrast” method described in sections 2.1 and 2.2 of the present paper.

ii) For nc materials, conventional HRTEM can be used to characterize perfect lattice dislocations and Shockley twinning partials while the ADF-HRSTEM have proved its ability to reveal the near core properties of residual Frank sessile dislocations by minimizing the contrast of the strong strain field surrounding this type of dislocations.

It was also demonstrated that, owing to the small grain size in nc materials, the total number and the nature of the dislocations located at TBs can be precisely determined and used for the improvement of the investigation of the dislocation/TB reactions. Such behaviour cannot be accomplished in coarse-grained materials because in most cases the TBs expand in the thicker part of the TEM foils.

The results also show that TBs act as barriers to dislocation motion as well as sources for dislocation storage and multiplication via specific TB/dislocation reactions with a positive impact on the strength-ductility balance in these materials. The reactions depend mainly on the SFE as well as on the nature of the incoming lattice dislocations. In-situ straining TEM experiments are under preparation for direct observation of the dislocation/TB reactions shown in the present work.

Acknowledgements This work was carried out in the framework of the IAP program of the Belgian State Federal Office for Scientific, Technical and Cultural Affairs, under Contract No. P6/24. The Titan 80-300 microscope used in this study was partially financed by the Hercules Foundation.

References

[1] Christian JW, Mahajan S. Deformation twinning. *Progress in Materials Science*. 1995;39:1-157

[2] Humphreys FJ, Hatherly S. Recrystallization and related annealing phenomena. New York: Pergamon; 1995.

[3] Gubicza J, Chinh NQ, Labar JL, Hegedus Z, Langdon TG. Twinning and dislocation activity in silver processed by severe plastic deformation. *Journal of Materials Science*. 2009;44:16561660

[4] Nieman GW, Weertman JR, Siegel RW. Mechanical behavior of nanocrystalline Cu and Pd. *Journal of Materials Research*. 1991;6:1012-1027

[5] Valiev RZ, Estrin Y, Horita Z, Langdon TG, Zehetbauer MJ, Zhu YT. Producing bulk ultrafine-grained materials by severe plastic deformation. *JOM*. 2006;58:33-39

[6] Chen MW, Ma E, Hemker KJ, Sheng HW, Wang YM, Cheng XM. Deformation twinning in nanocrystalline aluminum. *Science*. 2003;300:1275-1277

[7] Lu L, Shen YF, Chen XH, Qian LH, Lu K. Ultrahigh Strength and High Electrical Conductivity in Copper. *Science*. 2004;304:422-426

[8] Zhang X, Misra A, Wang H, Nastasi M, Embury JD, Mitchell TE, Hoagland RG, Hirth JP. Nanoscale-twinning-induced strengthening in austenitic stainless steel thin films. *Applied Physics Letters*. 2004;84:1096-1098

[9] Lu K, Lu L, Suresh S. Strengthening Materials by Engineering Coherent Internal Boundaries at the Nanoscale. *Science*. 2009;324:349-352

[10] Zhu YT, Narayan J, Hirth JP, Mahajan S, Wu XL, Liao XZ. Formation of single and multiple deformation twins in nanocrystalline fcc metals. *Acta Materialia.* 2009;57:3763-3770

[11] Yamakov V, Wolf D, Phillpot SR, Gleiter H. Dislocation–dislocation and dislocation–twin reactions in nanocrystalline Al by molecular dynamics simulation. *Acta Materialia*. 2003;51:4135-4147

[12] Sansoz F, Huang HC, Warner DH. An atomistic perspective on twinning phenomena in nano-enhanced fcc metals. *JOM*. 2008;60(9):79-84

[13] Afanasyev KA, Sansoz F. Strengthening in gold nanopillars with nanoscale twins. *Nano Letters*. 2007;7:2056-2062

[14] Hadfield RA. Hadfield manganese steel. *Science*. 1888;12:284-286

[15] Idrissi H, Renard K, Ryelandt L, Schryvers D, Jacques PJ. On the mechanism of twin formation in Fe–Mn–C TWIP steels. *Acta Materialia*. 2010;58:2464-2476

[16] Howie A, Whelan MJ. Diffraction contrast of electron microscope images of crystal lattice defects. *Proceedings of the Royal Society A*. 1962;267:206-230

[17] Silcock JM, Tunstall WJ. Partial dislocations associated with NbC precipitation in austenitic stainless steels. *Philosophical Magazine*. 1964;10:361-389

[18] Mori T, Fujita H. Dislocation reactions during deformation twinning in Cu-11at.% Al single crystals. *Acta Metallurgica.* 1980;28:771-776

[19] Cohen JB, Weertman J. A dislocation model for twinning in f.c.c. metals. *Acta Metallurgica*. 1963;11:996-998

[20] Béfahy S, Yunus S, Troosters M, Pardoen T, Bertrand P. Stretchable helical gold conductor on silicone rubber microwire. *Applied Physics Letters*. 2007;91:141911(1)- 141911(3)

[21] Haque MA, Saif MTA. Deformation mechanisms in free-standing nanoscale thin films: A quantitative in situ transmission electron microscope study. *Proceedings of the* National Academy *of Sciences*. 2004;101:6335-6340

[22] Yang DY, Lim TW, Son Y, Barlat F, Yoon JW. Gripless nanotension test for determination of nano-scale properties. *International Journal of Plasticity*. 2011;27:1527-1536

[23] Lacour S, Wagner S, Huang Z, Suo Z. Stretchable gold conductors on elastomeric substrates. *Applied Physics Letters*. 2003;82: 2404-2406

[24] Idrissi H, Wang B, Colla MS, Raskin JP, Schryvers D, Pardoen T. Ultrahigh strain hardening in thin palladium films with nanoscale twins. *Advanced Materials*. 2011;23:2119-2122

[25] Gravier S, Coulombier M, Safi A, Andre N, Boe A, Raskin JP, Pardoen T. New MEMS–Based micromechanical testing laboratory–Application to aluminium, polysilicon and silicon nitride. *Journal of Microelectromechanical Systems*. 2009;18:555-565

[26] Deshpande K, Meldon JH, Schmidt MA, Jensen KF. SOI-Supported Microdevice for Hydrogen Purification Using Palladium–Silver Membranes. *Journal of Microelectromechanical Systems*. 2010;19:402-409

[27] Colla MS, Wang B, Idrissi H, Schryvers D, Raskin JP, Pardoen T. High strength-ductility of thin nanocrystalline palladium films with nanoscale twins: on-chip testing and grain aggregate model. *Acta Materialia*. 2012;60:1795–1806

[28] Idrissi H, Turner S, Mitsuhara M, Wang B, Hata S, Coulombier M, Raskin JP, Pardoen T, Van Tendeloo G, Schryvers D. Point Defect Clusters and Dislocations in FIB Irradiated Nanocrystalline Aluminum Films: An Electron Tomography and Aberration-Corrected High-Resolution ADF-STEM Study. *Microscopy and Microanalysis*. 2011;17:983-990

[29] Jin ZH, Gumbsch P, Albe K, Ma E, Lu K, Gleiter H, Hahn H. Interactions between non-screw lattice dislocations and coherent twin boundaries in face-centered cubic metals. *Acta Materialia*. 2008;56:1126-1135

[30] Wang B, Idrissi H, Shi H, Colla MS, Michotte S, Raskin JP, Pardoen T, Schryvers D. Texture dependent twin formation in nanocrystalline thin Pd films. *Scripta Materialia*. 2012;66:866-871

[31] Wang B, Idrissi H, Galceran M, Colla MS, Turner S, Hui S, Raskin JP, Pardoen T, Godet S, Schryvers D. Advanced TEM investigation of the plasticity mechanisms in nanocrystalline freestanding palladium films with nanoscale twins. *International Journal of Plasticity*. In-press, http://dx.doi.org/10.1016/j.ijplas.2012.04.003